Contents lists available at ScienceDirect

Journal of Saudi Chemical Society

journal homepage: www.ksu.edu.sa

Original article

New benzotriazole-derived α-substituted hemiaminal ethers with enhanced cholinesterase inhibition activity: Synthesis, structural, and biological evaluations

Zain Maqsood Cheema [a,c], Muhammad Nisar [a], Humaira Yasmeen Gondal [a,*], Sami A. Alhussain [b,*], Magdi E.A. Zaki [b], Iain Coldham [c]

[a] Institute of Chemistry, University of Sargodha, Sargodha, Pakistan
[b] Department of Chemistry, College of Science, Imam Mohammad Ibn Saud Islamic University (IMSIU), Riyadh 13623, Saudi Arabia
[c] Department of Chemistry, University of Sheffield, Brook Hill, Sheffield S3 7HF, UK

ARTICLE INFO

Keywords:
Hemiaminal ethers
Benzotriazole
Cholinesterases
Alzheimer's Disease
(*R*)-menthol
(*R*)-fenchyl alcohol
Neurological disorders

ABSTRACT

A new series of benzotriazole-derived α-substituted hemiaminal ethers have been synthesized as human cholinesterase (hChE) inhibitors with enhanced activity. The synthesized compounds were extensively characterized by ^{1}H NMR and ^{13}C NMR spectroscopy, mass spectrometry, and SC-XRD studies. All the compounds demonstrated dual inhibition potential against acetyl and butylcholinesterases (AChE and BChE) in the *in-vitro* studies. Results revealed that compounds carrying the optically active (*R*)-menthol group demonstrated more activity than the bicyclic (*R*)-fenchol moiety. For instance, α-butyl-(*R*)-menthyl-benzotriazole derivative (**5a-iii**) exhibited the best AChE inhibition with an IC_{50} value of 44.03 nM, while its α-methyl analog (**5a-i**) showed promising results against BChE inhibition (IC_{50} = 80.74 nM). The molecular modeling study was carried out to assess the binding interactions with the target proteins to rationalize the structural–activity relationship. Subsequently, the stability of the protein–ligand complex was verified through molecular dynamics (MD) simulations. Pharmacokinetic and bioavailability parameters further supported the suitability of the new inhibitors as lead compounds for neurological disorders.

1. Introduction

Hemiaminal ethers represent a promising area of research in designing innovative therapeutic compounds for a broad spectrum of diseases. They are significant structural motifs of many biologically active natural products and synthetic pharmaceutical agents [1–6] (Fig. 1a). Their medicinal utilities are widely expanded as anti-cancer, anti-HIV, and anti-HCV agents. [7–10] They have also proved their effectiveness against cholinesterase inhibition for treating neurodegenerative issues.[11,12] Moreover, optically active hemiaminal ethers are of particular interest where the presence of stereogenic centers is considered responsible for their activities.[13–17].

Cholinergic signaling in the human body is regulated by a class of enzymes called cholinesterases (ChEs), which include butylcholinesterase (BChE) and acetylcholinesterase (AChE).[1–6] The abnormal concentration of cholinesterases (ChEs) in the body can cause many neuro-disorders, such as Parkinson's and Alzheimer's Disease.[3,4]As Alzheimer's disease (AD) advances, there is an observed increase in the activity of butyrylcholinesterase (BuChE) concurrent with a decline in brain acetylcholinesterase (AChE) levels [7]. This phenomenon can attributed to the sequence similarity between AChE and BuChE [8,9], which allows BuChE to hydrolyze acetylcholine (ACh) [7]. Cholinesterase inhibitors play a crucial role in regulating these cholinesterases to address the progression of these neurodegenerative disorders. With the global population aging, the prevalence of these debilitating conditions is escalating, emphasizing the pressing need for more efficacious therapeutic interventions. Numerous natural and synthetic inhibitors such as rivastigmine, tacrine, donepezil, pyridostigmine, and edrophonium (Fig. 1b), have been documented for their ability to modulate these enzymes [5,6,10–12]. However, these medications provide only symptomatic relief and often come with significant side effects. Therefore, the quest for novel cholinesterase inhibitors is not just about improving the

Peer review under responsibility of King Saud University. Production and hosting by Elsevier.

* Corresponding authors.
E-mail addresses: humaira.yasmeen@uos.edu.pk (H. Yasmeen Gondal), mezaki@imamu.edu.sa (M.E.A. Zaki).

https://doi.org/10.1016/j.jscs.2023.101746
Received 15 July 2023; Received in revised form 1 October 2023; Accepted 8 October 2023
Available online 12 October 2023

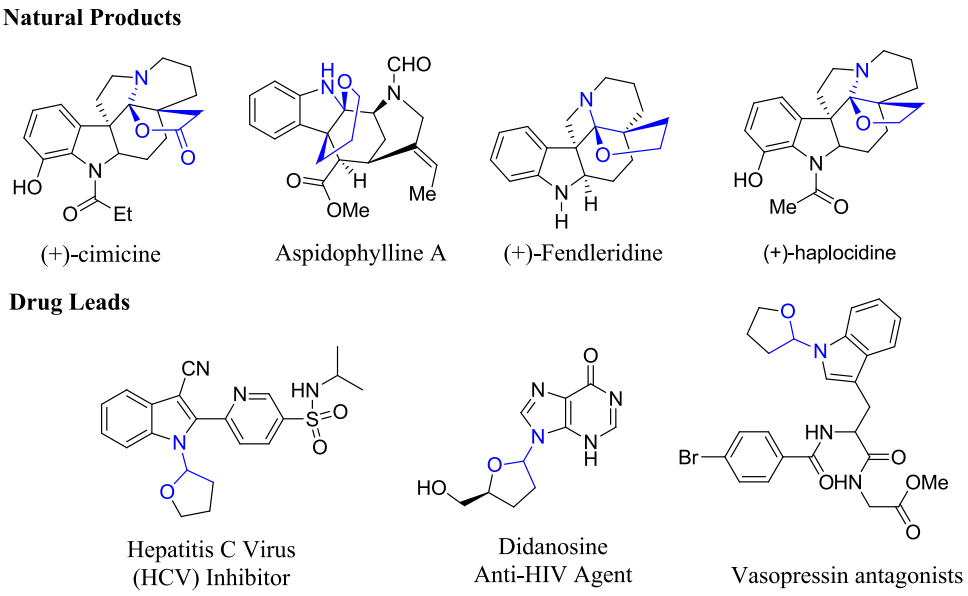

Fig. 1a. Some Representative medicinally important hemiaminal ethers.

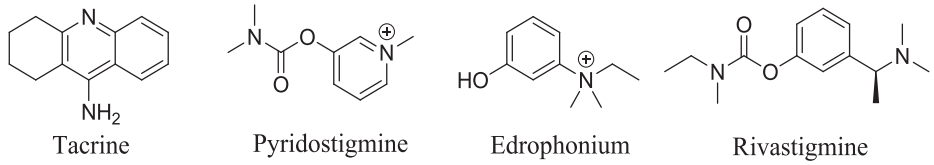

Fig. 1b. Selected examples of commercially available ChEs Inhibitors.

quality of life for millions of affected individuals but also about alleviating the growing socioeconomic burden associated with these diseases. Discovering new, simple, and cost-effective inhibitors can offer the understanding and management of neurogenerative disorders and the development of more targeted therapeutic interventions. As part of our ongoing research on alkoxymethylation, [15–23] we recently reported a new class of azole-derived hemiaminal ethers as promising acetylcholinesterase inhibitors.[23] These findings encouraged us to synthesize new synthetic analogs from this class to extend the structure–activity relationship in search of more potent inhibitors. Here, we designed a new class of α-substituted benzotriazole derived chiral hemiaminal ethers. We anticipate that the α-substitution and chiral alkoxy groups may allow the ligand to better conform to the chiral enzyme's cavity, where the benzotriazole ring facilitates significant π-π and π-alkyl interactions. Collectively, all of these factors may contribute to enhance the overall effectiveness of the ligand in its binding to the target protein. To access the target ligands, the charge stabilization ability of benzotriazole and the chirality of (*R*)-menthyl and (*R*)-fenchyl groups offer a significant synthetic utility. *In-vitro* and *in-silico* studies were performed to explore their potential against cholinesterases (ACh and BCh). Molecular modeling and molecular simulation studies demonstrated the stability of protein–ligand complex, whereas ADMET properties were studied to investigate the suitability of new compounds as drug leads. All-inclusive studies revealed that the α-substitutions on the previously synthesized alkoxymethyl benzotriazole derivatives effectively enhance the bioactivity of their parent hemiaminal ethers.

2. Materials and methods

All experiments were carried out under an argon atmosphere with oven-dried glassware and magnetic stirring. All solvents were obtained from the Grubbs dry solvent system (model: SPS-200–6 or SPS-400–6). Reactions were monitored on TLC plates Merck (silica gel 60 F254). Melting points were recorded on a Gallenkamp hot stage. IR spectra were measured on a Perkin Elmer Spectrum RX Fourier Transform IR System. Bruker Avance NMR III spectrometer was used for ^{1}H (400 MHz) and ^{13}C NMR (100 MHz) with deuterated chloroform as the solvent. Peak multiplicity is indicated as follows; s (singlet), d (doublet), t (triplet), q (quartet), and m (multiplet), and *J* values are given in Hertz. Specific rotations were calculated from optical rotations recorded on an AA-10 automatic polarimeter. X-ray crystal structures were obtained by a Bruker D8 Venture CMOS Photon 100. Mass spectra were measured by using Agilent Tech. 6530 LC/MS or Agilent Tech. 7200 GC/MS-Q-TOF.

2.1. General procedure for the synthesis of chiral alkoxymethyl benzotriazoles

To the stirred solution of benzotriazole (10 mmol) in dichloromethane (5 ml), diisopropyl ethyl amine (10 mmol) was added dropwise. The solution was allowed to stir for 30 min at room temperature followed by a slow addition of alkoxymethylchlorides[22](12 mmol). The reaction was allowed to reflux for 4 h, extracted with chloroform and the product was purified by column chromatography using hexane/ethyl acetate.

1-(((2-Isopropyl-5-methylcyclohexyl)oxy)methyl)-1H-benzo[d][1,2,3]triazole (**4a**):[32] White crystalline solid, m.p. 92–94 °C, Yield = 78 %; ν_{max}/cm^{-1}: 2954, 2868, 1451, 1376, 1266, 1172, 1075, 741. –106.6 (0.02, $CHCl_3$). ^{1}HNMR (400 MHz, $CDCl_3$) $\delta = 7.99$ (1H, d, J = 8), 7.63 (1H, d, $J = 8$), 7.45 (1H, t, $J = 8$), 7.34–7.28 (1H, m), 6.06 (1H, d, $J = 11.5$), 5.91 (1H, d, $J = 11.5$), 3.18 (1H, td, $J = 10.5, 4$), 2.02–1.99 (1H, m), 1.75–1.68 (1H, m), 1.57–1.40 (2H, m), 1.35–1.22 (2H, m), 1.13–1.08 (1H, m), 0.82 (3H, d, $J = 7$), 0.80–0.70 (2H, m), 0.63 (3H, d, $J = 7$), –0.09 (3H, d, $J = 7$). ^{13}CNMR (100 MHz, $CDCl_3$) $\delta = 146.3$, 132.8, 127.7, 124.2, 119.8, 109.9, 77.0, 74.4, 47.8, 39.7, 34.1, 31.2, 25.0, 22.7,

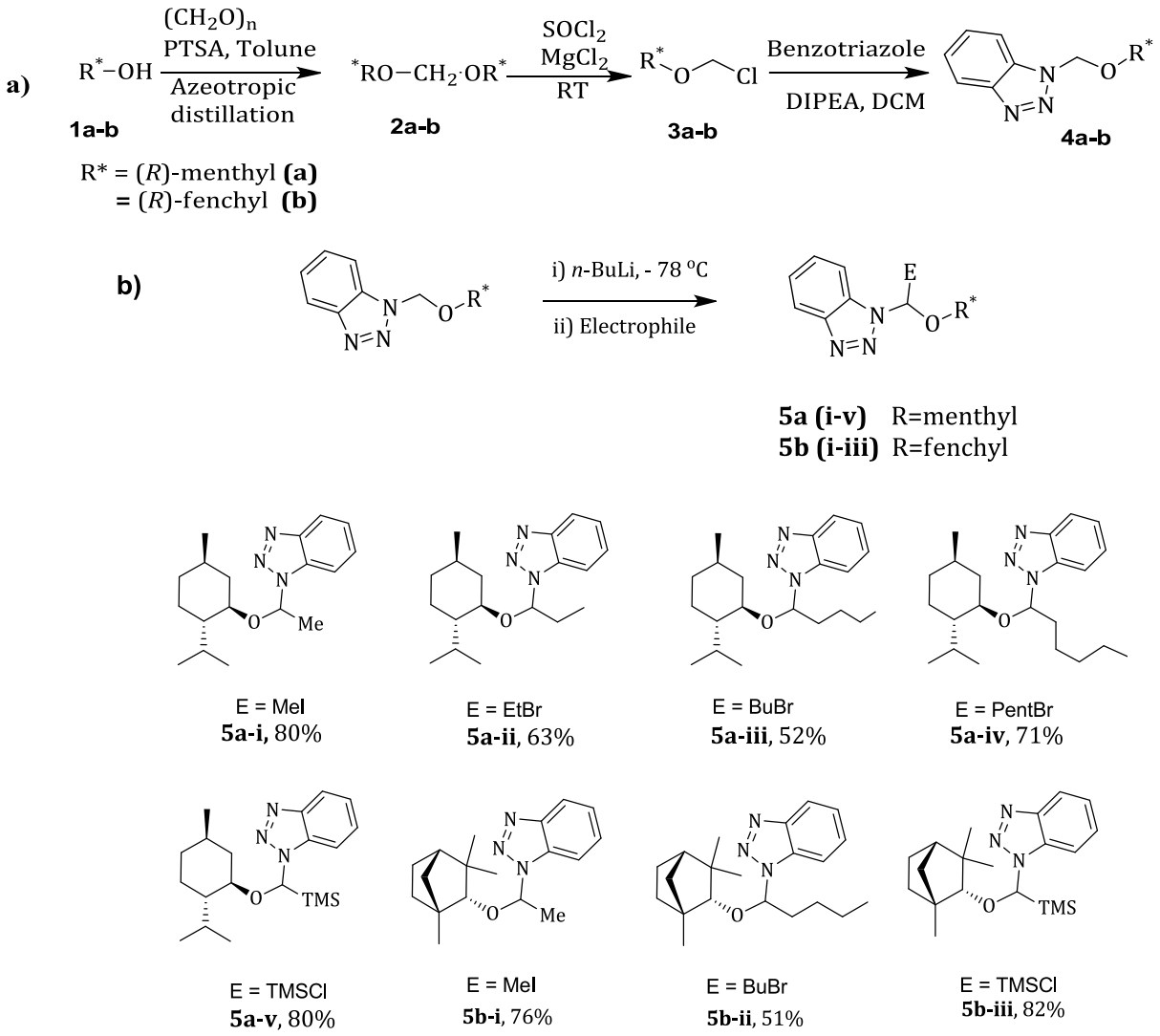

Scheme 1. Synthesis of α-substitedbenzotraiazole-based hemiaminal ethers.

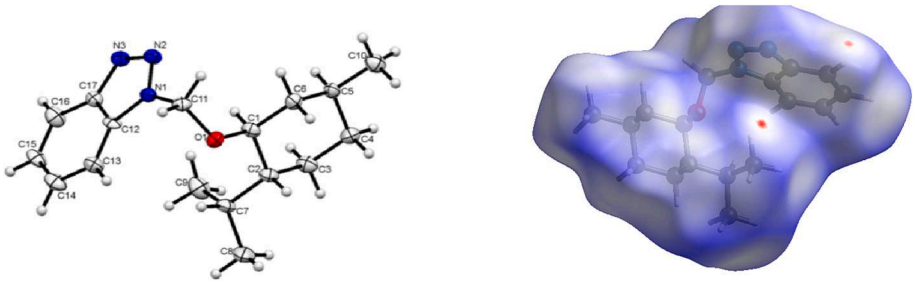

Fig. 2. ORTEP diagram (Left) and Hirshfeld surface (Right) of (R)-menthyloxymethyl benzotriazole **4a.**

22.2, 20.8, 14.8. HRMS (ESI) calculated for $C_{17}H_{25}N_3O$: 287.1998; found: 287.2003. CCDC 1855734.

1-[({1,3,3-Trimethylbicyclo[2.2.1]heptan-2-yl}oxy)methyl]-1,2,3-benzotriazole (**4b**): [32] m.p. 80–82 °C. Yield = 83 %; ν_{max}/cm^{-1}: 2950, 2872, 1493, 1375, 1270, 1089, 741. + 47.9 (0.02, $CHCl_3$).^{1}HNMR(400 MHz, $CDCl_3$) $\delta = 8.10$ (1H, d, $J = 8$), 7.72 (1H, d, $J = 8$), 7.54 (1H, t, $J = 8$), 7.42 (1H, t, $J = 8$), 6.01 (2H, ABq, $J = 11$), 3.27 (1H, s), 1.74–1.65 (2H, m), 1.62–1.61 (1H, m), 1.41–1.34 (2H, m), 1.05–0.92 (2H, m), 0.86 (3H, s), 0.74 (3H, s), 0.72 (3H, s). ^{13}CNMR (100 MHz, $CDCl_3$) $\delta = 146.5$, 132.8, 127.7, 124.3, 120.0, 110.2, 91.6, 77.7, 48.9, 48.5, 41.1, 39.1, 31.0, 25.9, 25.8, 20.9, 19.1. HRMS (ESI) calculated for $C_{17}H_{23}N_3O$: 285.1836; found 285.1840.

2.2. General procedure for α-substitution of benzotriazole based hemiaminal ethers

n-BuLi (2.5 M, 12 mmol) was added to the alkoxymethylated benzotriazole (10 mmol) in dry THF at –78 °C. After 10 min, the electrophile i.e. methyl iodide, ethyl bromide, butyl bromide, pentyl bromide, or trimethylsilyl chloride (10 mmol) in dry THF was added and the reaction

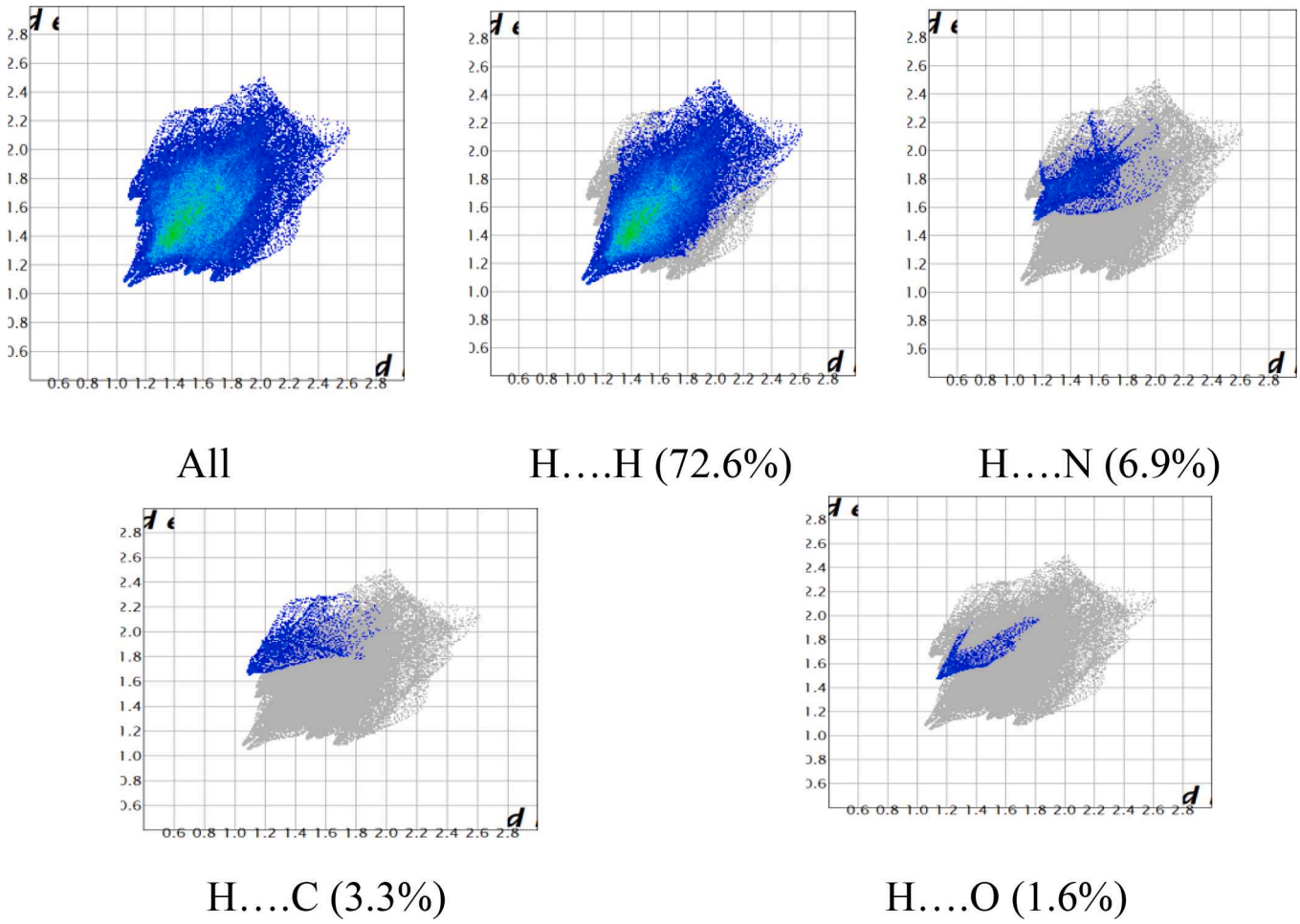

Fig. 3. 2D fingerprint plot of (*R*)-menthyloxymethyl benzotriazole **4a.**

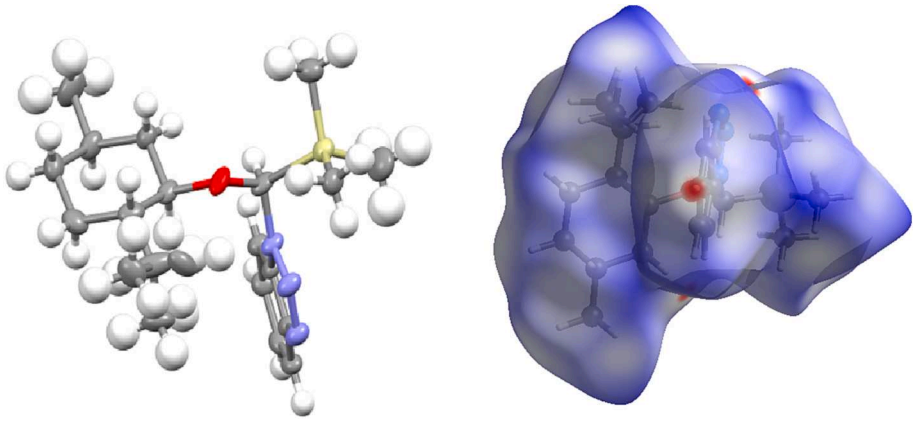

Fig. 4. ORTEP diagram (*Left*) and Hirshfeld surface (*Right*) of **5a-v.**

mixture was allowed to warm slowly to room temperature. Methanol was added and the solvent was evaporated. Purification by column chromatography on silica, eluting with petrol–EtOAc (95:5), gave the products.

1-(1-{[(1R,2S,5R)-2-Isopropyl-5-methylcyclohexyl]oxy}ethyl)-1,2,3-benzotriazole (**5a-i**): dr 1.1:1;ν_{max}/cm^{-1}: 2974, 2871, 1613, 1453, 1336, 1298, 1122, 1098, 771. ^{1}HNMR(400 MHz, $CDCl_3$) δ = 8.11–8.05 (1H, m), 7.81 (1H, d, J = 8), 7.51–7.47 (1H, m), 7.41–7.36 (1H, m), 6.46 (0.52H, q, J = 6.5, major isomer), 6.32 (0.48H, q, J = 6.5, minor isomer), 3.45 (0.48H, td, J = 10.5, 4.5), 2.98 (0.52H, td, J = 10.5, 4), 2.34–2.31 (0.52H, m), 2.26–2.21 (0.48H, m), 1.92 (1.45H, d, J = 6.5), 1.86 (1.55H, d, J = 6.5), 1.63–1.46 (2H, m), 1.34–0.62 (12H, m), 0.58 (1.45H, d, J = 6.5), –0.39 (1.55H, d, J = 6.5).^{13}CNMR(100 MHz, $CDCl_3$) δ = 147.1, 147.0, 131.3, 131.2, 127.25, 127.2, 124.1 (2C), 120.1 (2C), 111.7, 111.4, 88.1, 83.1, 81.0, 76.0, 48.9, 47.7, 41.5, 39.6, 34.2, 34.0, 31.3, 31.2, 25.8, 24.6, 23.0, 22.5, 22.3, 21.9, 21.4, 21.2, 21.1, 20.9, 16.3, 14.2.HRMS (ESI) calculated for $C_{18}H_{27}N_3O$: 301.2149; found: 301.2150.

1-(1-{[(1R,2S,5R)-2-Isopropyl-5-methylcyclohexyl]oxy}propyl)-1,2,3-benzotriazole (**5a-ii**): dr 2:1;ν_{max}/cm^{-1}: 2958, 2868, 1567, 1454,

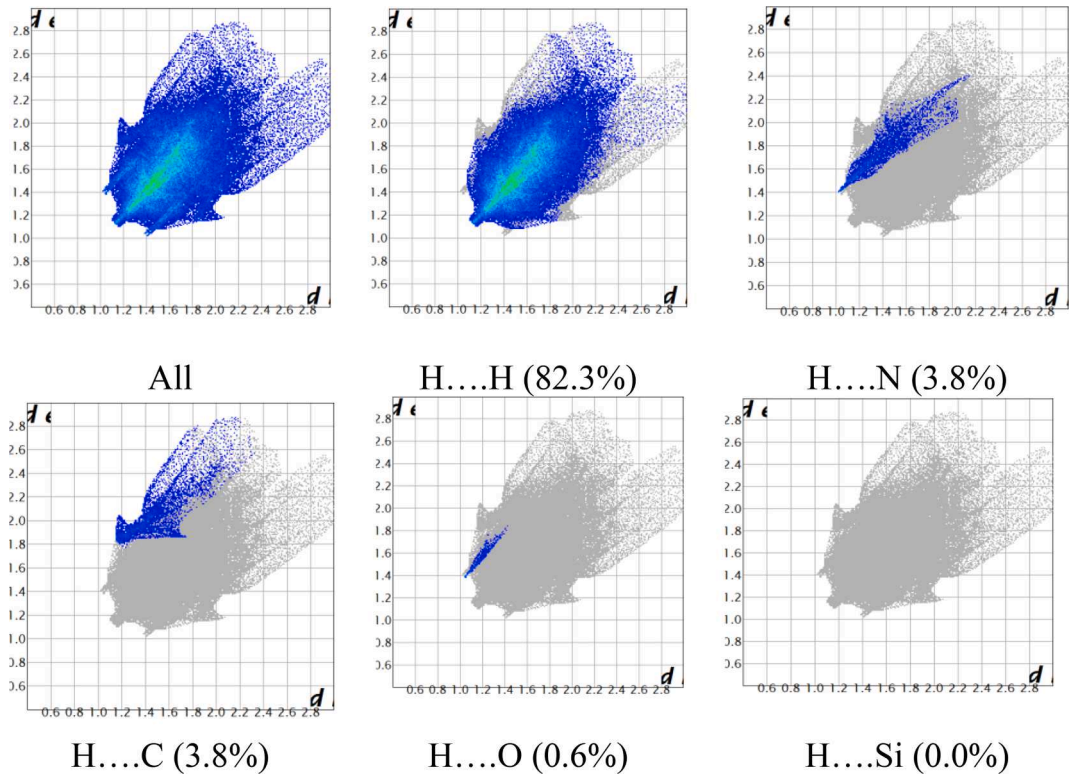

Fig. 5. 2D fingerprint plot of α-trimethylsilyl substituted (*R*)-menthyloxymethylbenzotriazole (**5a-v**).

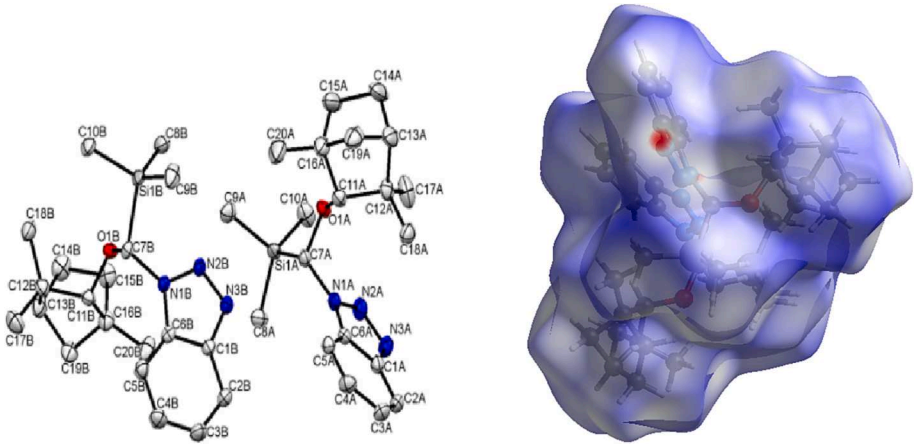

Fig. 6. ORTEP diagram (*Left*) and Hirshfeld surface (*Right*) of the co-crystallized **5b-iii.**

1113, 964, 745.^{1}HNMR(400 MHz, $CDCl_3$) δ = 8.10–8.06 (1H, m), 7.80 (1H, d, J = 8), 7.48–7.46 (1H, m), 7.42–7.37 (1H, m), 6.15 (0.67H, t, J = 7, major isomer), 6.05 (0.33H, t, J = 6.5, minor isomer), 3.46 (0.33H, td, J = 10.4, 4.5), 3.04 (0.67H, td, J = 11.0, 4.6), 2.41–2.25 (2H, m), 2.25–2.13 (1H, m), 1.86–1.79 (0.67H, m), 1.64–1.47 (2H, m), 1.41–1.05 (3.33H, m), 1.02–0.72 (9H, m), 0.68 (2H, d, J = 7), 0.57 (1H, d, J = 6.5), –0.42 (2H, d, J = 7). ^{13}CNMR (100 MHz, $CDCl_3$) δ = 147.0, 146.9, 131.4, 131.3, 127.1, 127.0, 124.1 (2C), 120.0 (2C), 111.7, 111.4, 93.1, 88.4, 81.3, 76.2, 48.8, 47.7, 41.3, 39.6, 34.3, 34.0, 31.3, 28.5, 27.7, 25.5, 24.6, 22.9, 22.5, 22.3, 21.9, 21.2, 20.9, 16.1, 14.6, 14.1, 9.6, 9.4. HRMS (ESI) calculated for $C_{19}H_{29}N_3O$: 315.2305; found: 315.2315.

1-(1-{[(1R,2S,5R)-2-Isopropyl-5-methylcyclohexyl]oxy}pentyl)-1,2,3-benzotriazole(**5a-iii**): dr 1.6:1;ν_{max}/cm^{-1}: 2954, 2876, 1563, 1450, 1258, 1105, 741. ^{1}HNMR (400 MHz, $CDCl_3$) δ = 8.10–8.06 (1H, m), 7.81 (1H, d, J = 8.5), 7.51–7.46 (1H, m), 7.42–7.37 (1H, m), 6.22 (0.62H, t, J = 7, major isomer), 6.12 (0.38H, t, J = 7, minor isomer), 3.46 (0.38H, td, J = 10.5, 4), 3.03 (0.62H, td, J = 10.5, 4.5), 2.37–2.25 (2H, m), 2.23–2.10 (1H, m), 1.86–1.79 (1H, m), 1.64–1.03 (9H, m), 1.01–0.82 (9.1H, m), 0.68 (1.9H, d, J = 7), 0.56 (1.1H, d, J = 7), –0.43 (1.9H, d, J = 7).^{13}CNMR(100 MHz, $CDCl_3$) δ = 147.0, 146.9, 131.4, 131.3, 127.15, 127.1, 124.1 (2C), 120.0 (2C), 111.7, 111.5, 91.8, 87.2, 81.2, 76.1, 48.9, 47.7, 41.3, 39.6, 34.9, 34.3, 34.2, 34.0, 31.3, 27.3, 26.9, 25.5, 24.6, 22.8, 22.5, 22.3, 22.15, 22.1, 21.9, 21.2, 20.9, 16.1, 14.1, 13.85, 13.8. HRMS (ESI) calculated for $C_{21}H_{33}N_3O$: 343.2618; found: 343.2635.

1-(1-{[(1R,2S,5R)-2-Isopropyl-5-methylcyclohexyl]oxy}hexyl)-1,2,3-benzotriazole (**5a-iv**): dr 1.8:1;ν_{max}/cm^{-1}: 2974, 2871, 1613, 1453,1336, 1298, 1122, 1014, 771.^{1}HNMR(400 MHz, $CDCl_3$) δ = 8.08–8.05 (1H, m), 7.80–7.78 (1H, d, J = 8), 7.49–7.44 (1H, m), 7.40–7.39 (1H, m), 6.21 (0.65H, t, J = 6.7, major isomer), 6.11 (0.35H, t, J = 6.5, minor isomer), 3.44 (0.35H, td, J = 10.5, 4.5), 3.02 (0.65H, td, J = 10.5, 4.5), 2.35–2.10 (3H, m), 1.84–1.79 (0.65H, m), 1.62–1.03

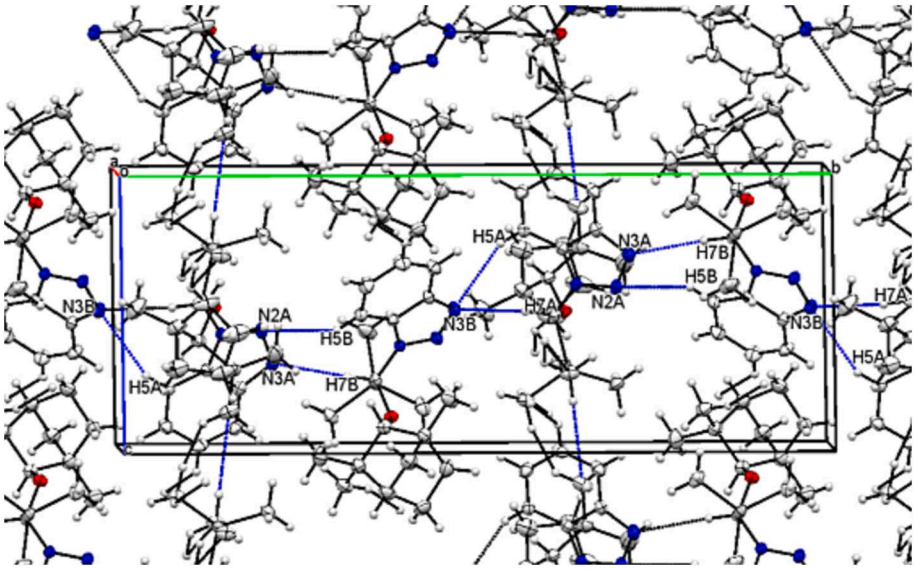

Fig. 7. Packing diagram of co-crystallized diastereomers **5b-iii.**

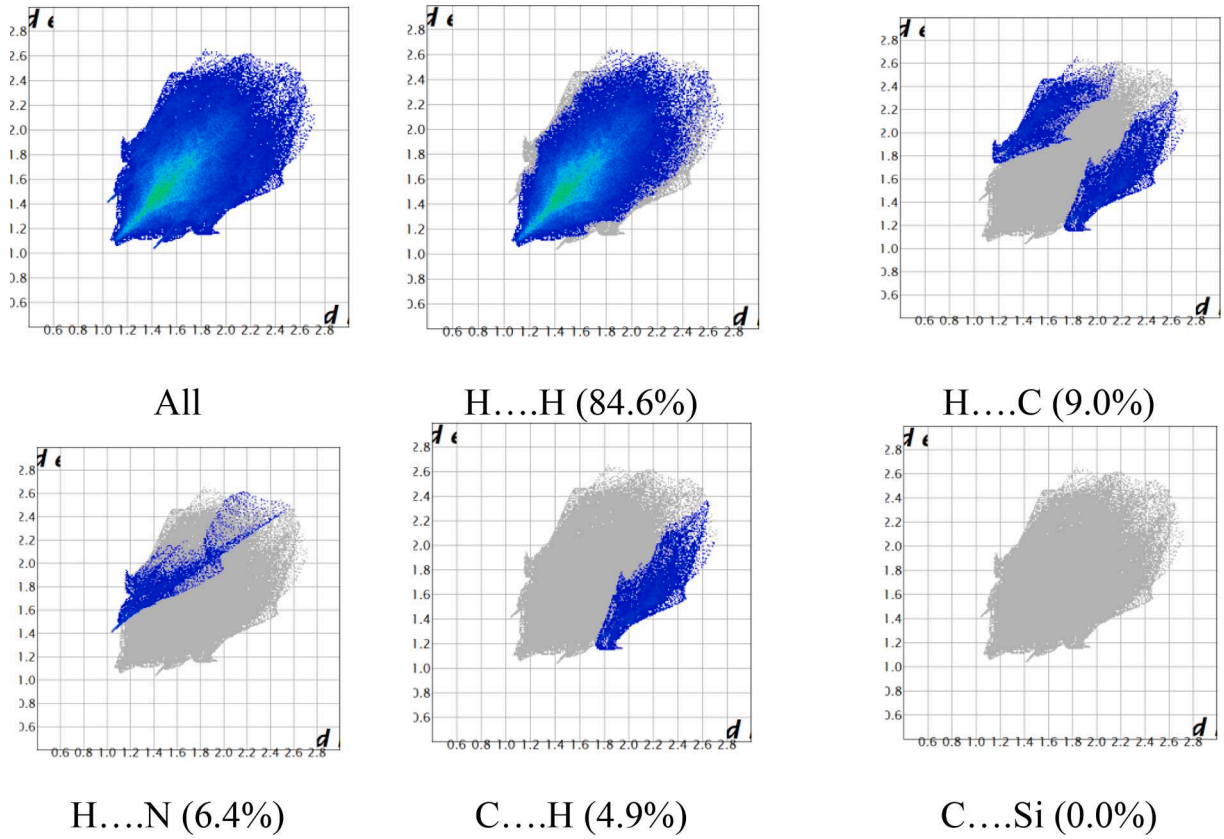

Fig. 8. 2D fingerprint plot of α-trimethylsilyl substituted (*R*)-fenchyloxymethylbenzotriazole (**5b-iii**).

(12.35H, m), 1.00–0.70 (8H, m), 0.67 (2H, d, $J = 7$), 0.55 (1H, d, $J = 6.5$), –0.42 (2H, d, $J = 6.5$). ^{13}CNMR (100 MHz, $CDCl_3$) $\delta = 147.0, 146.9, 131.5, 131.3, 127.2, 127.1, 124.1$ (2C), 120.0 (2C), 111.7, 111.4, 91.8, 87.2, 81.2, 76.1, 48.9, 47.6, 41.4, 39.6, 35.2, 34.4, 34.2, 34.0, 31.25, 31.2, 31.1, 25.5, 24.8, 24.6, 24.5, 23.9, 22.8, 22.5, 22.4, 22.35, 22.3, 21.9, 21.2, 20.9, 16.1, 14.1, 13.95, 13.9. HRMS (ESI) calculated for $C_{22}H_{35}N_3O$: 357.2775; found: 357.2778.

1-[(S)-{[(1R,2S,5R)-2-Isopropyl-5-methylcyclohexyl]oxy}(trimethylsilyl)methyl]-1,2,3-benzotriazole (**5a-v**): dr 6:1, data for major isomer: –100 (0.01, $CHCl_3$). m.p. 122–124 °C; ν_{max}/cm^{-1}: 2970, 2876, 1614, 1454, 1152, 1078, 745.^{1}HNMR(400 MHz, $CDCl_3$) $\delta = 8.06$ (1H, d, $J = 8$), 7.67 (1H, d, $J = 8$), 7.48 (1H, t, $J = 8$), 7.37 (1H, t, $J = 8$), 5.98 (1H, s, major isomer), 2.99 (1H, td, $J = 10.5, 4$), 2.31–2.28 (1H, m), 1.97–1.90 (1H, m), 1.52–1.47 (2H, m), 1.28–1.16 (2H, m), 0.98 (3H, d, $J = 6.5$), 0.93–0.74 (3H, m), 0.70 (3H, d, $J = 6.5$), 0.16 (9H, s), –0.28 (3H, d, $J = 6.5$).^{13}CNMR (100 MHz, $CDCl_3$) $\delta = 146.3, 133.3, 127.0, 123.8, 119.9, 110.7, 81.3, 77.6, 47.8, 39.3, 34.3, 31.4, 24.8, 22.8, 22.4, 20.9, 14.5, –3.1$.HRMS (ESI) calculated for $C_{20}H_{33}N_3OSi$: 382.2285;

Table 1
Cholinsterases inhibition by new α-substituted hemiaminal ethers.

Compounds			AChE		BChE	
No.	**Alkoxy Group**	**α-Substitution**	**IC_{50} (nM)**	**Ki (nM)**	**IC_{50} (nM)**	**Ki (nM)**
5a-i	(*R*)-menthyl	Me	52.91	35 ± 06	80.03	31 ± 40
5a-ii	(*R*)-menthyl	Et	54.28	38 ± 72	82.19	42 ± 71
5a-iii	(*R*)-menthyl	Bu	44.03	25 ± 90	109.20	63 ± 29
5a-iv	(*R*)-menthyl	Pent	60.39	48 ± 07	133.82	79 ± 47
5a-v	(*R*)-menthyl	TMS	66.48	52 ± 19	109.54	76 ± 3
5b-i	(*R*)-fenchyl	Me	80.74	59 ± 43	83.73	51 ± 8
5b-ii	(*R*)-fenchyl	Bu	76.57	49 ± 08	97.46	61 ± 21
5b-iii	(*R*)-fenchyl	TMS	79.92	55 ± 74	94.65	57 ± 09
Donepezil			62.09	37 ± 84	91.01	51 ± 34

found: 382.2286.CCDC 1855732.

1-(1-{[(1S,4S)-1,3,3-Trimethylbicyclo[2.2.1]heptan-2-yl]oxy} ethyl)-1,2,3-benzotriazole (**5b-i**): dr 1.1:1;ν_{max}/cm^{-1}: 2938, 2876, 1556, 1391, 1093, 995, 749. ^{1}HNMR (400 MHz, $CDCl_3$) δ = 8.09–8.05 (1H, m), 7.82–7.79 (1H, m), 7.51–7.45 (1H, m), 7.40–7.35 (1H, m), 6.26 (0.45H, q, J = 6.5, minor isomer), 6.21 (0.55H, q, J = 6.5, major isomer), 3.12 (0.45H, s), 2.95 (0.55H, s), 1.93 (1.3H, d, J = 6.5), 1.89 (1.7H, d, J = 6.5), 1.80–1.69 (2H, m), 1.64–1.28 (3H, m), 1.23 (1.7H, s), 1.14 (1.7H, s), 1.06 (1.3H, s), 0.96–0.88 (2H, m), 0.47 (1.3H, s), 0.32 (1.7H, s), 0.26 (1.3H, s). ^{13}CNMR (100 MHz, $CDCl_3$) δ = 147.0, 146.9, 131.15, 131.1, 127.1, 127.0, 124.1, 124.05, 120.1, 120.0, 111.8, 111.7, 91.8, 90.0, 88.1, 86.9, 49.4, 48.9, 48.5, 47.9, 41.3, 41.1, 39.6, 38.9, 31.7, 30.1, 26.1, 26.0, 25.9, 25.7, 21.0, 20.8, 20.7, 20.65, 20.2, 19.0. HRMS (ESI) calculated for $C_{18}H_{25}N_3O$: 299.1992; found: 299.1993.

1-(1-{[(1S,4S)-1,3,3-Trimethylbicyclo[2.2.1]heptan-2-yl]oxy}pentyl)-1,2,3-benzotriazole (**5b-ii**): dr 2.8:1;ν_{max}/cm^{-1}: 2958, 2876, 1458, 1364, 1089, 745. ^{1}HNMR (400 MHz, $CDCl_3$) δ = 8.10–8.04 (1H, m), 7.89 (1H, d, J = 8), 7.51–7.45 (1H, m), 7.41–7.36 (1H, m), 6.09–5.97 (1H, m), 3.09 (0.27H, s, minor isomer), 2.91 (0.73H, s, major isomer), 2.47–2.13 (2H, m), 1.82–1.61 (3H, m), 1.50–1.24 (6.75H, m), 1.13 (2.25H, s), 1.09 (2.25H, s), 0.95–0.82 (5H, m), 0.49 (0.75H, s), 0.34 (2.25H, s), 0.21 (0.75H, s). ^{13}CNMR (100 MHz, $CDCl_3$) δ = 147.0 (2C), 131.3, 131.2, 127.1, 127.0, 124.0 (2C), 120.1, 120.0, 111.8 (2C), 91.9, 91.4, 90.6, 89.8, 49.5, 49.0, 48.6, 47.9, 41.3, 41.1, 39.6, 39.0, 34.2, 34.0, 31.7, 30.1, 27.4, 26.9, 26.2, 26.0, 25.95, 25.8, 22.2, 22.15, 21.3, 20.8, 20.4, 19.1, 13.8, 13.75. HRMS (ESI) calculated for $C_{21}H_{31}N_3O$: 341.2462; found: 341.2466.

1-({[(1S,4S)-1,3,3-Trimethylbicyclo[2.2.1]heptan-2-yl]oxy} (trimethylsilyl)methyl)-1,2,3-benzotriazole (**5b-iii**): dr 1.5:1, m.p. 146–148 °C; ν_{max}/cm^{-1}: 2970, 2876, 1614, 1454, 1375, 1078, 745. ^{1}HNMR(400 MHz, D6-DMSO) δ = 8.07–8.03 (1H, m), 7.95–7.90 (1H, m), 7.61–7.56 (1H, m), 7.43–7.37 (1H, m), 5.96 (0.6H, s, major isomer), 5.85 (0.4H, s, minor isomer), 2.98 (0.4H, s), 2.76 (0.6H, s), 1.78–0.79 (7H, m), 1.24 (1.2H, s), 1.08 (1.8H, s), 1.03 (1.8H, s), 0.33 (1.2H, s), 0.19 (1.8H, s), 0.16 (3.5H, s), 0.11 (5.5H, s), –0.06 (1.2H, s).^{13}CNMR (100 MHz, D6-DMSO, major isomer only listed, two quaternary C could not be observed) δ = 150.1, 138.9, 132.6, 129.2, 124.4, 116.3, 99.1, 95.9, 53.7, 53.4, 45.1, 36.6, 30.7, 26.3, 25.0, 2.2.HRMS (ESI) calculated for $C_{20}H_{31}N_3OSi$: 357.2231; found: 357.2226.CCDC 1855733.

2.3. In-vitro cholinesterase inhibition studies

In-vitro inhibition study of the synthesized hemiaminal ethers was carried out by slight modification in Ellman's spectrophotometric method. [22,23] A mixture of phosphate buffer (60 µL, KH_2PO_4/KOH, pH 7.7), inhibitor (10 µL) and enzyme (10 µL, 0.015 unit/well for AChE and BChE separately, was preincubated at 37 °C for 10 min. Then, acetylthiocholine chloride, or butylthiocholine iodide 1 mM (10 µL) was added to the enzyme reaction mixture. Later, 0.5 mM DTNB (10 µL) was added as coloring reagent. Absorbance (at 405 nm) was measured using microplate readers after 20 min of incubation at 37 °C. Donepenzil was used as a positive control. All experiments were carried out in triplicate at three different concentrations and percentage inhibition was calculated. Compounds with high inhibition ability (>50 %) against cholinesterases were further evaluated for the IC_{50}. Enzyme kinetic studies were carried [24] to understand the mode of inhibition for the most potent derivatives **5a-iii** for AChE and **5a-i** for BChE at different concentrations of inhibitor (0, 0.5, 1.0, 2.0 nM) and substrate (0, 0.087, 0.175, 0.35 and 0.7 µM). Lineweaver–Burk plot was generated by using GraphPad PRISM (8.4.3) [25].

Table 2
Binding affinities (Kcal/mol) of α-substituted benzotriazole-based hemiaminal ethers against selected proteins of cholinesterase.

Compounds			AChE		BChE
No.	**Alkoxy Group**	**α-Substitution**	**6o4x**	**2h7c**	**1P0I**
5a-i	(*R*)-menthyl	Me	−10.1	−8.7	−10.1
5a-ii	(*R*)-menthyl	Et	−10.1	−8.8	−10.1
5a-iii	(*R*)-menthyl	Bu	−10.3	−9.0	−9.8
5a-iv	(*R*)-menthyl	Pent	−10.1	−8.2	−9.6
5a-v	(*R*)-menthyl	TMS	−7.5	−6.1	−7.0
5b-i	(*R*)-fenchyl	Me	−8.7	−9.0	−10.1
5b-ii	(*R*)-fenchyl	Bu	−8.9	−8.2	−9.7
5b-iii	(*R*)-fenchyl	TMS	−7.6	−7.9	−9.5
Donepezil			−9.7	−10.4	−8.9

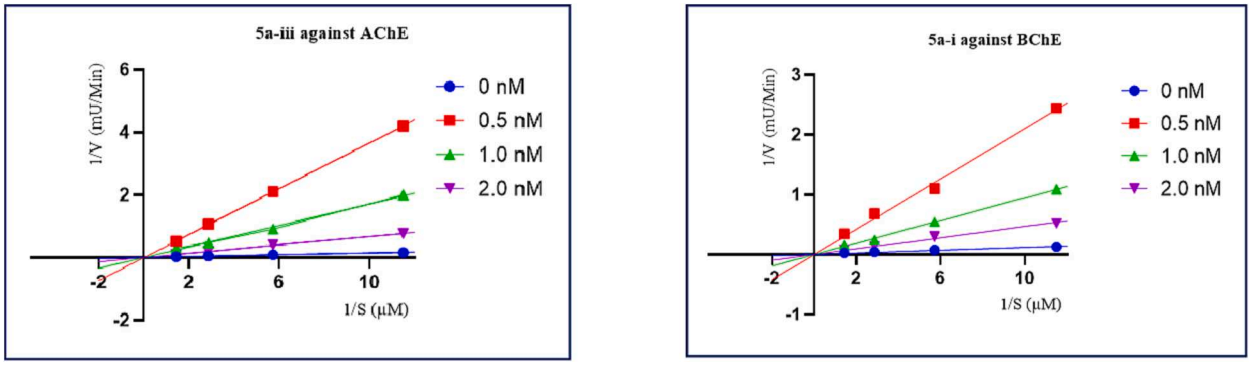

Fig. 9. Kinetic studies of most potent 5a-iii against AChE (*left*) and 5a-i against BChE (*right*).

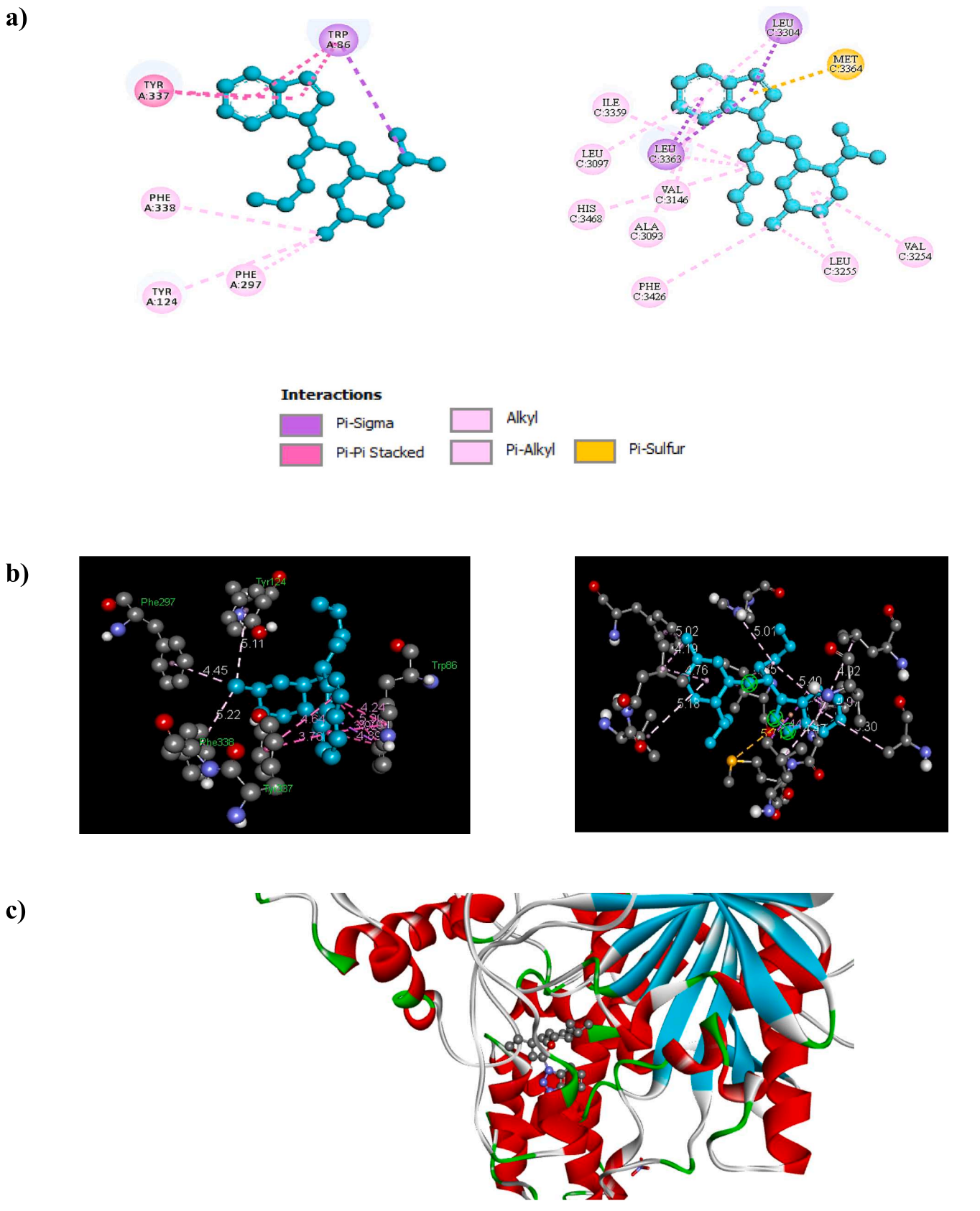

Fig. 10. Molecular docking interactions of α-butyl menthyloxymethyl benzotriazole (**5a-iii**) **a)** 2D Interactions **b)** 3D interactions with AChE proteins 6o4x (*Left*) and 2h7c (*Right*) **c)** Protein-ligand complex with AChE Protein 6o4x.

Table 3
Comparative analysis of interactions of synthesized ligand, native ligand, and standard drug with protein 6o4x.

Ligand	Amino acids in chain A	Interaction Type	Distance (Å)
5a-iii	PHE:338,PHE:297, TYR:337, TRP:124, TRP:86	π-alkyl, π-alkyl, π-π stacked	5.21, 5.12, 4.44, 4.89, 4.59, 4.58, 3.74, 3.93,
Donepezil	TRP:286,PHE:297, TYR:337,TRP:341, TRP:86, ARG:296	C–H bond, π-alkyl, π-π stacked, π-Alkyl	5.32, 5.33, 5.04, 5.02, 4.92, 4.59, 3.41, 3.28
9AA	HIS:447, TYR:337, TRP:86	π-π stacked, H-bond	5.01, 5.47, 4.61, 4.42, 4.2

Table 4
Featured pharmacokinetic parameters of the hit compound **5a-i** and **5a-iii.**

No.	Properties	Results	
		5a-i	5a-iii
1.	Molecular Mass (g/mol)	301.43	343.51
2.	Number of rotatable bonds	4	7
3.	Hydrogen Bond donor	0	0
4.	Hydrogen Bond acceptor	3	3
5.	Topological Polar Surface Area ($A^{\circ 2}$)	39.94	39.94
6.	Skin Permeation (Log Kp) cm/s	−4.56	−3.78
7.	Molar Refractivity	90.64	105.06
8.	Lipophilicity (Log Po/w – XLOGGP3)	5.04	6.50
9.	Lipinski's Rule violation	0	1
10	Gestor-intestinal absorption	High	High
11.	Human Oral Bioavailability	0.55	0.55
12.	Blood Brain Barrier	+0.8000	+0.8000
13.	VDss (log L/kg)	0.26	0.155
14.	Total Clearance (log ml/min/kg)	1.111	1.212
15.	Renal OCT2 substrate	No	No
16.	LD_{50} (mg/kg)	120	120
17.	Toxicity Class	III	III

2.4. In-silico cholinesterase inhibition studies

The protein data bank was searched for the human ACh and BCh enzymes. Fourteen different proteins (seven for acetylcholine esterases/carboxylesterases and seven for butylcholineesterases) were downloaded from the RCSB protein data bank. Discovery Studio Visualizer [26] was used to save the chemical structures in pdb format. The proteins were downloaded from RCSB protein data bank in pdb format and were prepared by using autodock tools [27]. The proteins were saved in pdbqt format after removal of water molecules followed by addition of polar hydrogens and Kollman charges to balance the protein. The ligands were also saved in pdbqt format by using autodock tools. Auto dock vina and CB-Dock2 [28] were used to carry out docking studies and Discovery Studio Visualizer were employed to evaluate the results. Pharmacokinetic parameters and physicochemical properties were evaluated by online portals Protox-II [29], SwissADME [30] and pkCSM-biosig [31].

The output file generated through docking of selected ligand and protein converted into complex file in PyMol [32] and then used for generating protein and ligand topologies. Ligand topology is created by uploading the Mol2 file in SwissParam [33] online server. Protein topology, after trimming the chain with which ligand is showing interaction, was created by applying CHARM36 forcefield and TIP3P water model in GROMACS version 2020 [34] installed in Ubuntu 20.04. Both topologies were then complexed together, solvated after adding a decahedral box and system was neutralized by adding six sodium ions. This was followed by equilibrating the complex by minimizing the energy and then applying an Md run of 20 ns at constant pressure (1 atm) and temperature (300 K). After the completion of simulation, the trajectory file was analyzed through different in-built tools in GROMACS including gmx_rms, gmx_rmsf, gmx_gyrate, gmx_hbond, and gmx_energy for calculating RMSD (root mean square deviation), RMSF (root mean square fluctuation), Rg (radius of gyration), number of hydrogen bonds, Coulombic and Lennard-Jones interaction energies. VMD [35] and UCSF Chimera [36] was used for visualizing the trajectories and creating snapshots.

3. Results and discussion

3.1. Chemistry

The development of effective methods for the preparation of substituted hemiaminal ethers is a synthetic challenge for organic chemists. They have been reported by nucleophilic substitution of α-halo ethers, α-amination of ethers, and metal-catalyzed hydroamination of enols.[29–31] Recently, we have synthesized [23] some azole-derived hemiaminal ethers carrying chiral alkoxy part based on (*R*)-menthyl and (*R*)-fenchyl groups in three steps (Scheme 1a**).***Bis*-menthyloxymethanes (**2a-b**) were prepared by the condensation of formaldehyde with (*R*)-menthol (**1a**) and (*R*)-fenchyl alcohol (**1b**).[23] Chlorination of acetals with a combination of $SOCl_2/MgCl_2$ provided the corresponding α-halo ether (**3a-b**).Further, nucleophilic substitution with benzotriazole in the presence of DIPEA provided the corresponding alkoxymethyl benzotriazoles (**4a-b**) in good yields. [23] For current studies, we decided to substitute the α-position of the prepared hemiaminal ethers (**4a-b**), where the presence of benzotriazole moiety of anion-stabilizing ability provides an intriguing opportunity for the required functionalization.

To introduce the substitution at α-carbon, a series of experiments were performed to find the best conditions for α-lithiation of **4a** followed by electrophilic quench with alkyl halide (**Table S20,** *Supplementary Information*). Under the optimized condition, reaction of alkoxymethyl benzotriazole derivatives (**4a-b**) with *BuLi* (1.2 Eq) in THF at −78 °C provided the target α-substituted benzotriazole derivatives (Scheme 1b). The synthesized hemiaminal ethers [**5a(i-v)-5b(i-iii)**] were characterized by ^{1}H, ^{13}C NMR, Mass and XRD analysis.

3.2. Single crystal-XRD and Hirshfeld surface analysis

Compounds **4a**, **5a-v**, and **5b-iii** were obtained in the crystalline form and their structures were ultimately confirmed by single crystal XRD studies. In addition, Hirshfeild surface analysis was performed to observe the type of nonbonding interactions exists in the crystal lattice.

Menthyloxymethylated benzotriazole derivative (**4a**) was isolated as a white crystalline solid and SC-XRD confirmed the structure as 1-(1-{[(1R,2S,5R)-1-(2-Isopropyl-5-methylcyclohexyl)oxy)methyl)-1H-benzo[d][1,2,3]triazole. The structural parameters of **4a** revealed that the compound is crystallized in the monoclinic crystal system with a space group of $P2_1$. Interestingly an upfield methyl signal was observed at −0.3 ppm in the NMR spectrum of **4a** (*See supplementary information*), due to the anisotropic shielding of the benzotriazole ring as seen in the ORTEP diagram (Fig. 2, ***Left***).

Hirshfeld surface analysis was used to provide the quantitative knowledge of inter-molecular interaction based on d_{norm} property of the molecules and the distance of the atom (internal, di and external, de). The analysis was visualized by adjusting the color scale range from −0.039 (red) to 1.8579 (blue) Å, in the Crystal Explorer program (version 21.5). The red color shows the interatomic contact site (Fig. 2**,4,6** ***Right***), whereas 2D fingerprint plot quantifies the overall contribution of the intermolecular interactions, H….H (72.6 %), H….N (6.9 %), H….C (3.3 %) and H….O (1.6 %) towards the crystal lattice stability of the **4a** (Fig. 3). Likewise, the trimethylsilyl substituted derivative **5a-v** was also isolated as a crystalline solid. The structural parameters of 1-[(S)-{[(1R,2S,5R)-2-Isopropyl-5-methylcyclohexyl]oxy}(trimethylsilyl)methyl]-1,2,3-benzotriazole (**5a-v**) revealed that the compound has orthorhombic crystal system with space group of $P2_1$ (Fig. 4).

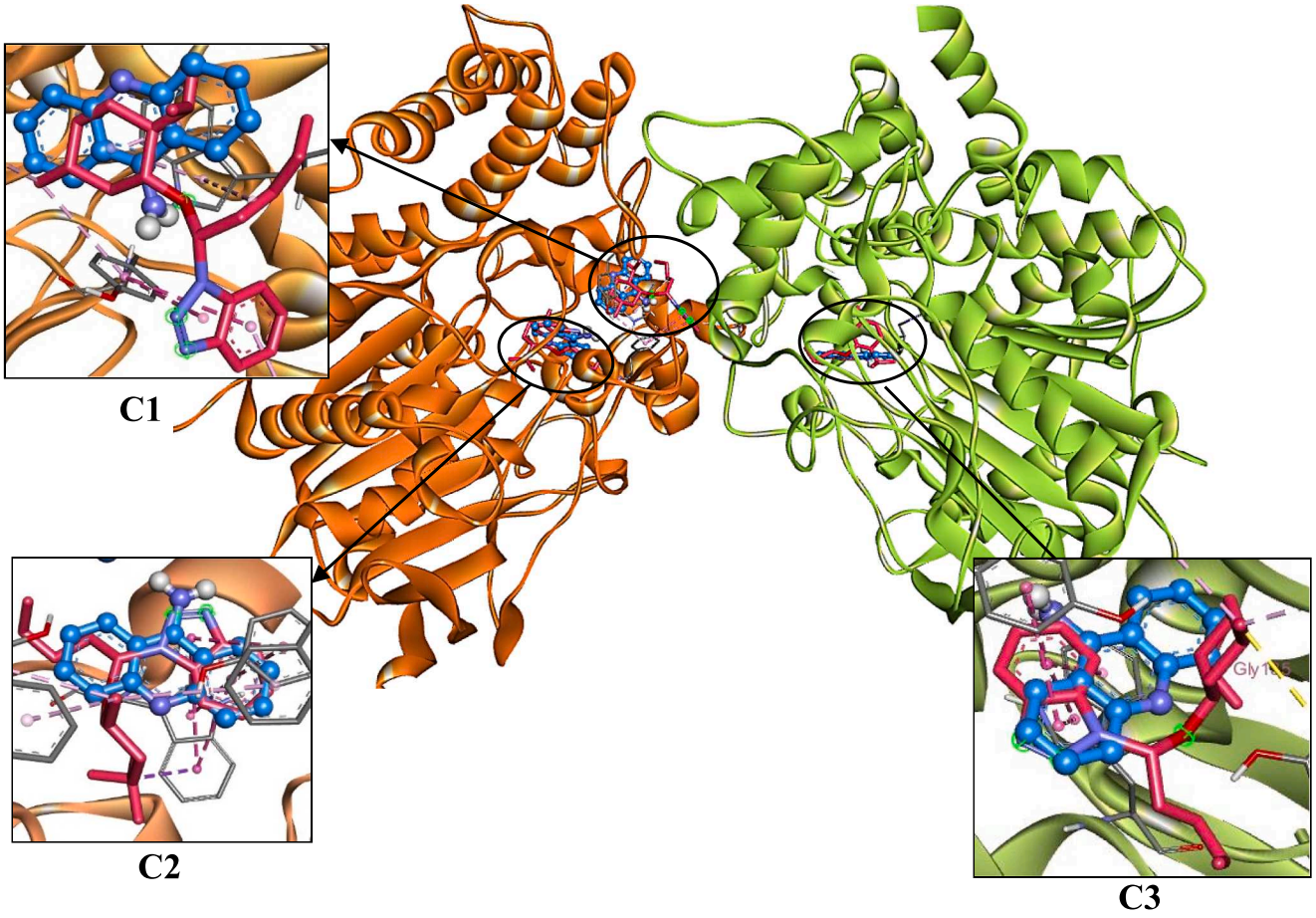

Fig. 11. 3D Demonstration of multiple docking results of 5a-iii and 9-aminoacridine with 6o4x.

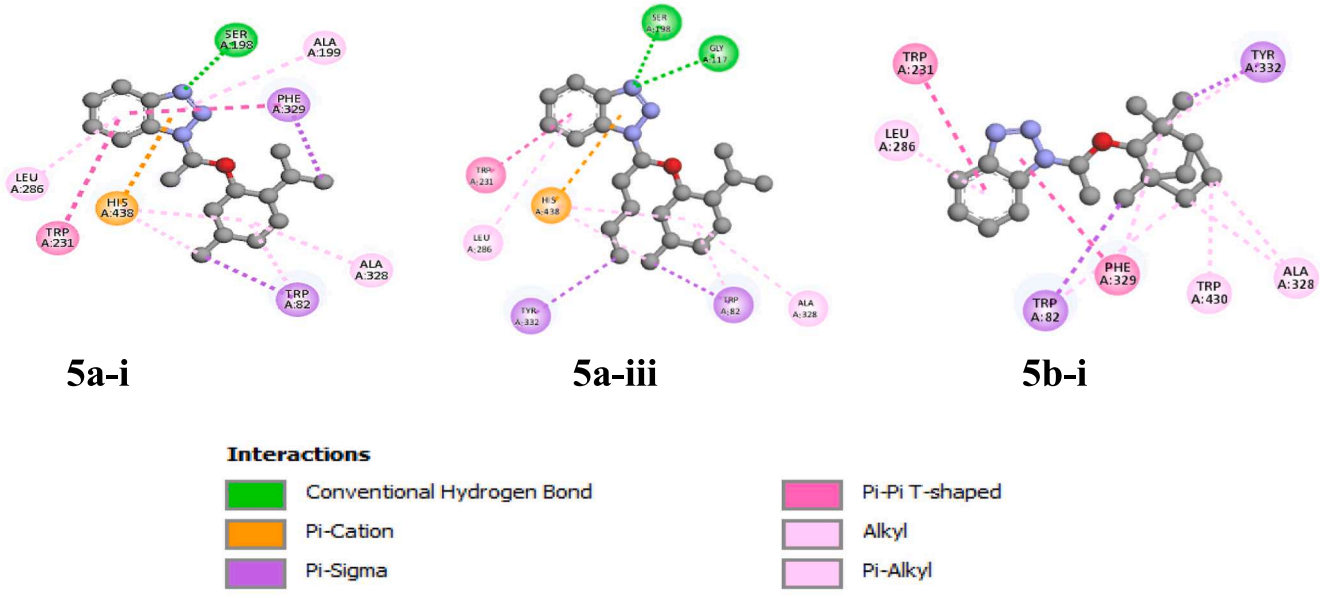

Fig. 12. Molecular docking interactions with BChE protein 1P0I **a)** 2D Interactions of **5a-i**, **5a-iii,** and **5b-i b)** Protein-ligand complex of (**5a-i**).

Whereas, the 2D fingerprint plot of 1-[(S)-{[(1R,2S,5R)-2-Isopropyl-5-methylcyclohexyl]oxy}(trimethylsilyl)methyl]-1,2,3-benzotriazole (5a-v) showed H….H (82.3 %), H….N (3.8 %), H….C (3.8 %) and H….O (0.6 %) intermolecular contribution towards lattice stability (Fig. 5). The 2D fingerprint plot showed that the significant interactions responsible for crystal packing in 5a-v are H…H interactions. Interestingly, the fenchyl analog 1-({[(1S,4S)-1,3,3-Trimethylbicyclo- [2.2.1] heptan-2-yl]oxy}(trimethylsilyl)methyl)-1,2,3-benzotriazole (**5b-iii**)

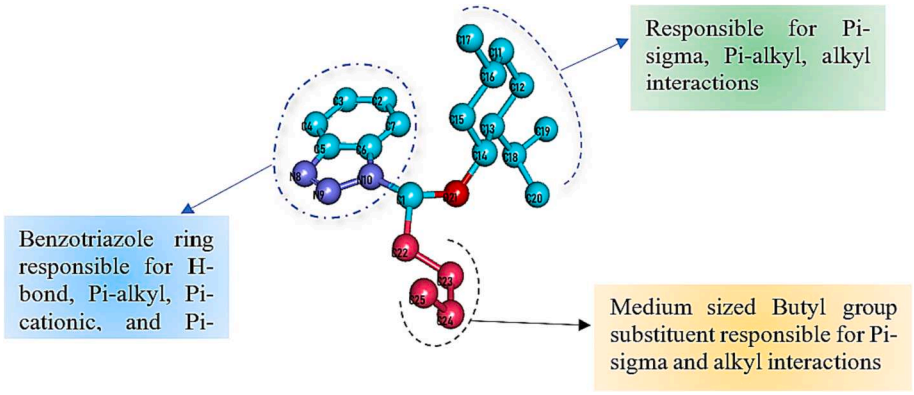

Fig. 13. Structural analysis of the synthesized compounds involving in the target inhibition.

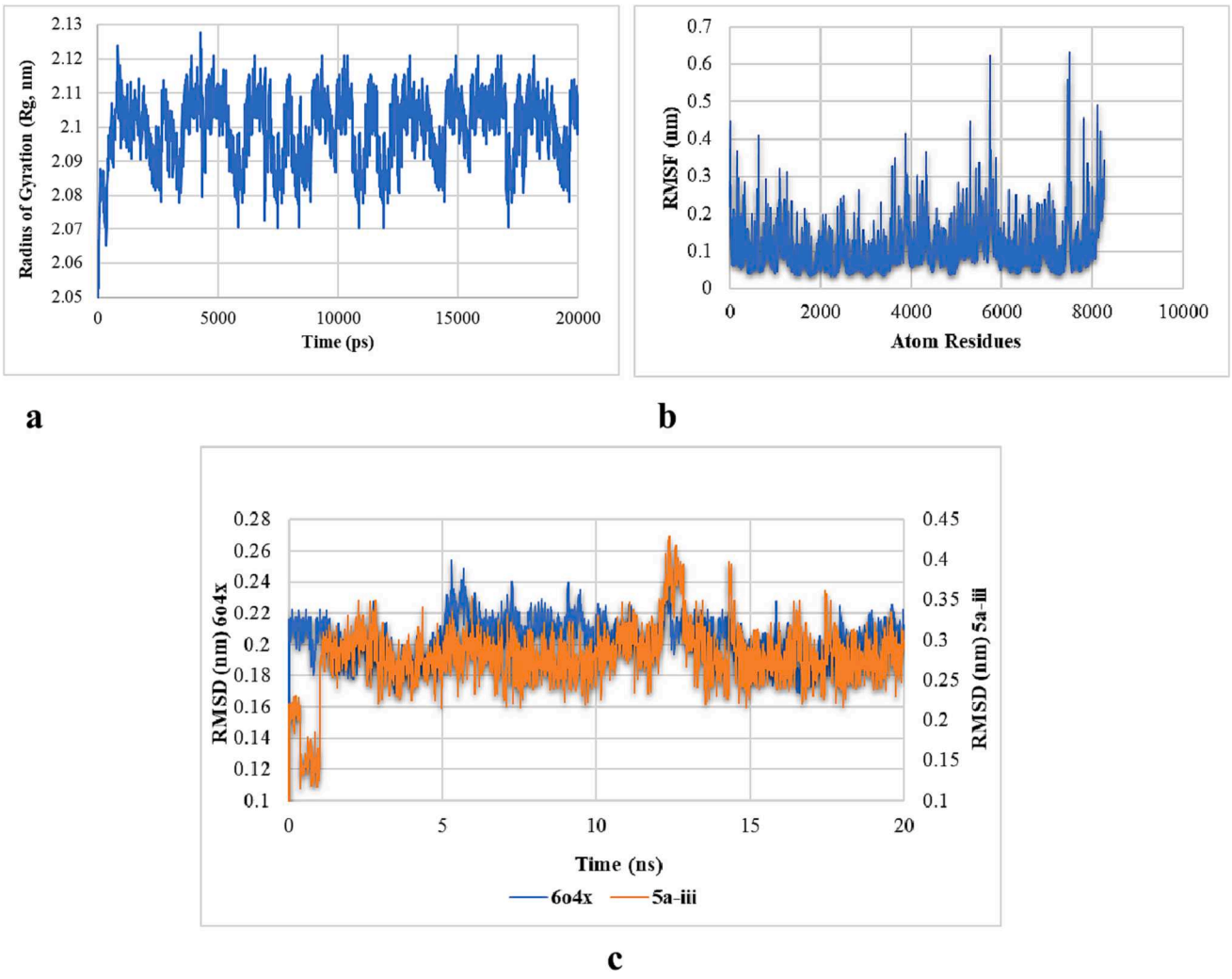

Fig. 14. Graphical representation of Radius of gyration and RMSF of protein, and RMSD of 6o4x and 5a-iii.

was isolated as co-crystal and single crystal X-ray analysis revealed that two molecules are in one asymmetric unit (Fig. 6).

The packing diagram (Fig. 7) shows the tetrahedral geometry with space group $P2_1$ and exists in two independent molecules A and B having two Si atoms in a unit cell. There are four asymmetric molecules of the complex in a unit cell showing secondary interactions. One such possible interaction occurs between a nitrogen atom of the triazole and a proton on a methyl group attached to the Si atom, providing stability to the complex diastereomeric mixture. Likewise, as per 2D fingerprint plot of 1-({[(1S,4S)-1,3,3-Trimethylbicyclo[2.2.1]heptan-2-yl]oxy}(trimethylsilyl)methyl)-1,2,3-benzotriazole (**5b-iii**) the contribution of interaction to the overall crystal lattice measured by 2D fingerprint plot revealed the H….H (84.6 %), H….C (9.0 %), H….N (6.4 %) and C….H (4.9 %) intermolecular contribution towards lattice stability (Fig. 8). Similar to α-silyl substituted ether 5a-v, the 2D fingerprint plot of substituted ether 5b-iii also showed that the significant interactions

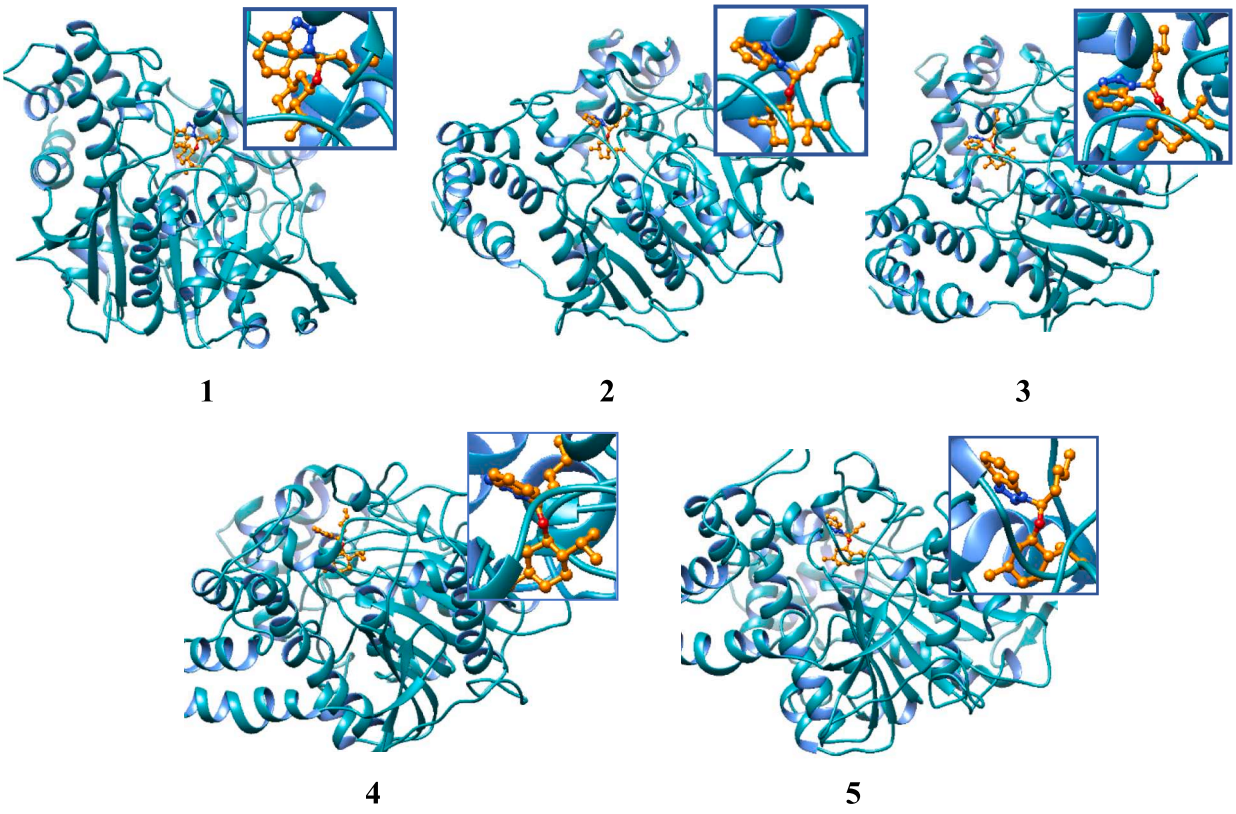

Fig. 15. Snapshots of **6o4x-5a-iii** complex during MD simulation.

responsible for crystal packing are H…H interactions.

3.3. In-vitro cholinesterases inhibition studies

All the synthesized compounds [**5a(i-v)** and **5b(i-iii)**] were subjected to in-vitro cholinesterase inhibition studies targeting both acetylcholinesterase and butyrylcholinesterase. Notably, these compounds demonstrated favorable inhibitory potential when compared to their parent hemiaminal ethers as well as the standard drug, donepezil. The results presented in Table 1 indicate that the activity of the compounds depends upon the specific chiral alkoxy group and the presence of α-substitution. Generally, it was observed that hemiaminal ethers containing the (*R*)-menthyloxymethyl group (**5a**) displayed superior inhibitory properties compared to their fenchyloxy counterparts (**5b**). Furthermore, compounds featuring a moderately sized α-alkyl group, such as butyl (**5a-iii**), exhibited the highest AChE activity, with an IC_{50} value of 44.03 nM. In contrast, compounds with smaller groups like methyl or ethyl (**5a i-ii**) or sterically demanding substitutions like pentyl or trimethyl silyl (**5a iv-v**) demonstrated comparatively lower activity (Table 1). Likewise, when assessing the inhibitory capabilities of the synthesized hemiaminal ethers against butylcholinesterase (BChE), compounds featuring the menthyloxy chiral component exhibited more promising outcomes. Specifically, compound **5a-i** displayed maximum inhibition capacity, with IC_{50} values of 80.03 nM (Table 1). These findings align with our earlier study, where we reported that compounds containing the menthol ring exhibit higher inhibitory potential than those containing the bicyclic fenchol moiety [23].

The kinetic studies of the most potent hit compounds, 5a-iii against AChE and 5a-i against BuChE were performed at various concentrations of inhibitor (0, 0.5, 1.0, 2.0 nM) and substrate (0, 0.087, 0.175, 0.35 and 0.70 μM). (Fig. 9 demonstrated the initial velocity of the reaction at different concentrations in the form of Lineweaver–Burk plots [24], where competitive inhibition was observed in both cases. These results effectively demonstrate that newly synthesized α-substituted hemiaminal ethers have remarkable inhibition potential against target enzymes and can considered for further studies as prospective candidates for the treatment of neurogenerative diseases. We anticipate that the presence of chiral alkoxy groups can offer significant binding with chiral proteins, the presence of α-substituted linear chains helps the ligand to best fit in the enzyme cavity through π-alkyl interactions, while the benzotriazole ring is responsible for π-π stacking.

3.4. In-silico cholinesterase inhibition studies

3.4.1. Molecular docking studies against different cholineasterase enzymes

To analyze the binding interaction of new α-substituted benzotriazole-derived hemiaminal ethers with cholinesterases (AChE and BuChE) molecular docking studies were carried out. The protein databank was searched for cholinesterase proteins and human acetylcholinesterase proteins 6o4x, 2h7c, and human butylcholinesterase protein 1P0I were selected. The docking results of all the synthesized compounds [**5a (i-v)** and **5b (i-iii)**] showed effective binding with selected proteins (Table 2).

The results revealed that the α-substituted derivatives carrying menthyl group **5a (i-iv)** exhibited high binding affinity (B.E. > -10.0 Kcal/mol) with receptor 6o4x as compared to the standard drug (-9.7 Kcal/mol). α-Butyl menthyloxymethyl benzotriazole (**5a-iii**) showed the maximum interactions with both proteins (B.E. −10.3 and −9.0 Kcal/mol). Different π-alkyl, π-π-stacking, and π-σ interactions were found to be involved with chain A of 6o4x (Fig. 10a, ***Left***) and π-alkyl interactions with chain C of protein 2h7c (Fig. 10a, ***Right***). In the case of interactions between ligand 5a-iii with receptor protein 6o4x, amino acids PHE:297, TYR:124, and PHE:338 were observed to be involved in π-alkyl interactions with a distance of 4.45, 5.11, and 5.22 Å. Similarly, 5a-iii also displayed significant interactions with protein 2h7c, where amino acids LEU:3255, PHE:3426, and VAL:3254 showed π-alkyl interactions with the menthol ring. The α-butyl group demonstrated alkyl-alkyl interactions with LEU:3363 and ILE:3359 with a distance of 5.40 and 4.85

Ao, and π-alkyl with HIS:3368 with 5.01Ao. Moreover, the benzotriazole ring in the ligand showed different π-stacking such as π-alkyl and π-σ interactions with various amino acid residues like LEU:3304, LEU:3363, and π-sulfur interactions with sulfur-containing amino acid MET:3364 (Fig. 10b, Right).

Further, a comparative analysis with the native ligand of protein 6o4x authenticated that **5a-iii** demonstrated significant interaction within the protein's active site. Docking 9-aminoacridine (the native ligand) with 6o4x revealed a lower docking score (9.2 kcal/mol) in comparison to the synthesized ligand **5a-iii** (-10.3 kcal/mol). The 2D representation (Fig. 10) evident that the hit compound 5a-iii, standard drug donepezil, and native ligand 9AA all interacted with the same amino acids (TYR: 337 and TRP: 86) in chain A through π-π interactions. 9AA also interacted with His:447, while the **5a-iii** additionally interacted with other amino acids, namely PHE: 297, PHE: 338, and TYR: 124. A detailed examination of the distances between the amino acid residues revealed that **5a-iii** is positioned in closer proximity to the protein's active site (Table 3).

9-aminoacridine found to posses distinct active site pockets within the protein. Multiple docking experiments were performed with both ligands (9AA and 5a-iii) in three additional site pockets (two in chain B and one in Chain A) by Discovery Studio Visualizer and CB Dock2. Results revealed that the hit compound exhibited stronger binding interactions with all three active sites within the protein (Table 4, Figure 11). It was observed that, among the three active sites, both ligands exhibited significant binding interactions with the C2 and C3 pockets i.e. −10.2 to 10.3 Kcal/mol for the hit compound and −9.0 to −9.2 Kcal/mol for native ligand (Table S24: *Supplementary Information*Information). Notably, the benzotriazole ring in **5a-iii** displayed an interaction pattern that closely resembled the hydrophobic rings of the native ligand 9AA, resulting in a high binding affinity. The presence of the alkyl substituent on **5a-iii** contributed to enhanced stability, as the presence of the butyl group caused the two ring systems to become perpendicular, which can effectively mask repulsive forces, resulting in a higher docking score. However, both 9-aminoacridine (9AA) and hemiaminal **5a-iii** exhibited lower binding scores (-7.1 to −7.6 Kcal/mol) in the C1 pocket. This phenomenon could also be attributed to a conformational change in the orientation of the ligand within the C1 pocket (Figure 11). Therefore, it can be inferred that the interactions responsible for establishing a protein–ligand binding are predominantly hydrophobic in nature.

In order to confirm the high inhibition potential of the hit compound, **5a-iii** was further docked with five other human AChE proteins, where the binding energy was observed between −8.6 to 9.7 Kcal/mol (Table S25: *Supplementary Information*).

The results from the acetylcholinesterase inhibition encouraged us to expand our studies to include human butyrylcholinesterase (1P0I). Remarkably, the hit compound **5a-iii** displayed a favorable binding affinity of −9.8 kcal/mol, higher than the donepezil (-8.9 Kcal/mol). Moreover, other synthesized hemiaminal ethers [**5a(i-ii)** and **5b(i)**] showed excellent binding affinity (>-10.0 Kcal/mol) with the receptor protein 1P01 (Table 2). The visualization of docking results revealed that compound **5a-i** demonstrates many prominent interactions such as π-alkyl, π-σ, π-π T-shape, and π-cation along with conventional hydrogen bonding with chain A of the receptor 1P0I. The amino acid residue Trp:82 showed π-σ and π-alkyl interactions with the menthyl part of the 5a-i. Whereas, benzotriazole ring was found to involve in π-π T-shape interactions with amino acid residue Trp:231, Phe:329, Leu:286, and His:438, and π-cation interactions along with hydrogen bonding with His:438 and Ser:198, respectively. Additionally, only the butyl group showed Pi-sigma interaction with TYR: 332 among these three (Fig. 12).

Both menthyloxy (**5a-i)** and fenchyloxy analogs **(5b-i)** demonstrated significant interactions such as π-alkyl, π-σ, and π-π T-shape interactions with different amino acid residues of Chain A of the receptor 1P0I (Fig. 12). The interactions of the active compounds **5a i-ii** and **5b-i** were further evaluated with other BChEs proteins (Table S26: *Supplementary Information*).

A comprehensive structural-activity analysis unveiled the role of specific groups in the synthesized compounds responsible for particular interactions within the protein residues (Fig. 13). For instance, the benzotriazole ring is found to be involved in many hydrophobic interactions, such as π-alkyl, π-cationic, and π-sigma interactions. Moreover, the chiral moiety in the molecules demonstrates π-alkyl, alky-alkyl, and π-sigma interactions. The O-CH group between the benzotriazole and chiral auxiliary serves as a linker, providing the necessary spacing between the two components. Additionally, the type and size of the alkyl group on the alpha carbon influenced binding affinity in many ways. For instance, medium-sized groups, like butyl, provide favorable conformational orientation to develop stable complexes.

The promising results from the enzyme inhibitory assay and docking studies have led us to conclude that the synthesized hemiaminal ethers hold significant potential for acetylcholinesterase inhibition. Molecular dynamics simulation further validated the stability of the complex between the hit compound **5a-iii** and the protein receptor (6o4x). Several parameters, including root mean square deviation (RMSD), root mean square fluctuations (RMSF), and radius of gyration (Rg), were calculated by analyzing the MD data to elucidate the dynamic interactions within the protein–ligand complex (Fig. 14). The post-simulation analysis revealed that 5a-iii forms a stable complex with 6o4x as ligand remaining inside the protein throughout the simulation. The average RMSD values were 0.22 nm for protein and 0.31 nm for 5a-iii. A slight increase to 0.41 nm at about 12 ns indicates a slight instability during this period relative to the rest of the simulation time. However, the overall RMSD values for both the ligand and protein remained below 1, indicating the stability of the complex. Moreover, Rg (Radius of gyration) was plotted against time, where a constant value of 2.1 nm suggests the compactness of the complex. The RMSF (root mean square fluctuations) value was observed at less than 0.5 nm except for a small variation for two residue points, suggesting a well-structured protein–ligand complex with minimal distortion. (Fig. 14).

Snapshot demonstration in Fig. 15 of the simulation process showed that the ligand maintained its conformation without significant changes throughout the entire simulation. In addition, the gmx_hbond script analysis confirmed the absence of hydrogen bonding between the protein and the ligand, thus validating the results obtained from the docking studies. In summary, the molecular dynamics (MD) simulation analysis revealed the formation of a stable complex between the protein and the ligand. This stability was supported by an average short-range Coulomb energy value of −21.9 KJ/mol and a Lenard-Jones (LJ) energy of −188.2 KJ/mol. The combined contribution of these two energy components resulted in a total interaction energy of −210.1 KJ/mol, further confirming the stability of the complex.

In short, *in-silico* studies were found in line with *in-vitro* studies, where α-butyl menthyloxymethyl benzotriazole **5a-iii** was found efficient AChE inhibitor and α-methyl derivative **5a-i** was found active against BChE. Both hit compounds (**5a-i** and **5a-iii**) were further subjected to physicochemical and pharmacokinetics evaluation and ADMET studies. Results displayed in Table 4, demonstrate the suitability of these compounds for further investigations as drug leads, where zero violation for 5a-i and one violation for 5a-iii was observed according to Lipinski rule. Molecular weight, solubility parameters, and structural features are all in favor of compounds' suitability as drug candidates except number of rotatable bonds in 5a-iii. Similarly, the Low Topological Polar Surface Area (TPSA) of 39.94 $A^{\circ 2}$ for each compound signified the good blood–brain penetration ability of the molecules. Additionally, the compounds exhibited high gastrointestinal absorption and human oral bioavailability scores, with no interactions as OCT2 substrates, further supporting their potential as drug leads for further study.

4. Conclusion

A new series of substituted benzotriazole-derived hemiaminal ethers

carrying a chiral alkoxy group of menthol and fenchol are successfully synthesized. *In-vitro* and *in-silico* studies were extensively employed to explore their potential against inhibition of cholinesterases. Results identified (*R*)-menthyl derivatives **5a-i** and **5a-iii** as the most effective compounds against BChEs and AChE inhibition. Molecular docking analyses helped in evaluating the roles of benzotriazole and menthol ring systems, as well as the impact of alkyl substituents on binding affinity. The results disclosed that the α-substitution significantly enhanced the inhibitory potential of the alkoxymethyl benzotriazoles. Molecular dynamics simulations further confirmed the stability of the protein–ligand complex with a total interaction energy of −210.1 kJ/mol. Pharmacokinetics and ADMET drug-likeness parameters supported the bioactivity and bioavailability of the synthesized hemiaminal ethers. Given their straightforward and efficient synthesis, these novel hemiaminal ethers hold substantial promise for the cost-effective development of medications targeting Alzheimer's disease (AD).

Funding statement

This work was supported and funded by the Deanship of Scientific Research at Imam Mohammad Ibn Saud Islamic University (IMSIU) (grant number IMSIU-RG23049). HEC Pakistan has supported the visit of Z.M.C at Sheffield University, UK under the HEC-IRSIP program.

Declaration of Competing Interest

The authors declare that they have no known competing financial interests or personal relationships that could have appeared to influence the work reported in this paper.

Acknowledgments

We are thankful to Craig C. Robertson, University of Sheffield, Brook Hill, Sheffield, UK, for performing SC-XRD and Shanza Munir, University of Sargodha, Pakistan for conducting the MD Simulation.

Appendix A. Supplementary material

Supplementary data to this article can be found online at https://doi.org/10.1016/j.jscs.2023.101746.

References

[1] İ. Gulçin, M. Abbasova, P. Taslimi, et al., Synthesis and biological evaluation of aminomethyl and alkoxymethyl derivatives as carbonic anhydrase, acetylcholinesterase and butyrylcholinesterase inhibitors, J. Enzyme Inhib. Med. Chem. 32 (2017) 1174–1182.
[2] F. Özbey, P. Taslimi, İ. Gülçin, et al., Synthesis of diaryl ethers with acetylcholinesterase, butyrylcholinesterase and carbonic anhydrase inhibitory actions, J. Enzyme Inhib. Med. Chem. 31 (2016) 79–85.
[3] A. Blokland, Acetylcholine: a neurotransmitter for learning and memory? Brain Res. Rev. 21 (1995) 285–300.
[4] Kocak, R., E. T. Akın, P. Kalın, et al., 2015. Month 2015 Synthesis of Some Novel Norbornene-Fused Pyridazines as Potent Inhibitors of Carbonic Anhydrase and Acetylcholinesterase.
[5] R.J. Obaid, N. Naeem, E.U. Mughal, et al., Inhibitory potential of nitrogen, oxygen and sulfur containing heterocyclic scaffolds against acetylcholinesterase and butyrylcholinesterase, RSC Adv. 12 (2022) 19764–19855.
[6] R.J. Obaid, E.U. Mughal, N. Naeem, et al., Pharmacological significance of nitrogen-containing five and six-membered heterocyclic scaffolds as potent cholinesterase inhibitors for drug discovery, Process Biochem. 120 (2022) 250–259.
[7] G.F. Makhaeva, N.P. Boltneva, S.V. Lushchekina, et al., Synthesis, molecular docking and biological evaluation of N, N-disubstituted 2-aminothiazolines as a new class of butyrylcholinesterase and carboxylesterase inhibitors, Bioorg. Med. Chem. 24 (2016) 1050–1062.
[8] A. Maryamabadi, A. Hasaninejad, N. Nowrouzi, et al., Application of PEG-400 as a green biodegradable polymeric medium for the catalyst-free synthesis of spiro-dihydropyridines and their use as acetyl and butyrylcholinesterase inhibitors, Bioorg. Med. Chem. 24 (2016) 1408–1417.
[9] D.O. Ozgun, C. Yamali, H.I. Gul, et al., Inhibitory effects of isatin Mannich bases on carbonic anhydrases, acetylcholinesterase, and butyrylcholinesterase, J. Enzyme Inhib. Med. Chem. 31 (2016) 1498–1501.
[10] N. Khunnawutmanotham, N. Chimnoi, P. Saparpakorn, et al., Synthesis and anti-acetylcholinesterase activity of scopoletin derivatives, Bioorg. Chem. 65 (2016) 137–145.
[11] G.L. Ellman, K.D. Courtney, V. Andres Jr, et al., A new and rapid colorimetric determination of acetylcholinesterase activity, Biochem. Pharmacol. 7 (1961) 88–95.
[12] A. Mumtaz, M. Shoaib, S. Zaib, et al., Synthesis, molecular modelling and biological evaluation of tetrasubstituted thiazoles towards cholinesterase enzymes and cytotoxicity studies, Bioorg. Chem. 78 (2018) 141–148.
[13] R. Kaur, S. Chaudhary, K. Kumar, et al., Recent synthetic and medicinal perspectives of dihydropyrimidinones: A review, Eur. J. Med. Chem. 132 (2017) 108–134.
[14] Z. Liu, Z. Zhang, W. Zhang, et al., 2-Substituted-1-(2-morpholinoethyl)-1H-naphtho [2, 3-d] imidazole-4, 9-diones: Design, synthesis and antiproliferative activity, Bioorg. Med. Chem. Lett. 28 (2018) 2454–2458.
[15] Z.M. Cheema, H.Y. Gondal, H. Siddiqui, et al., Solvent free synthesis of 1-alkoxy-phosphonium chlorides for stereoselective multipurpose vinyl ethers, Phosphorus Sulfur Silicon Relat. Elem. 195 (2020) 37–42.
[16] Z.M. Cheema, H.Y. Gondal, A.R. Raza, et al., Nucleophilic phenylation: a remarkable application of alkoxymethyltriphenylphosphonium salts, Mol. Divers. 24 (2020) 455–462.
[17] H.Y. Gondal, Z.M. Cheema, A.R. Raza, et al., α-alkoxyalkyl triphenylphosphonium salts: Synthesis and reactions, Curr. Org. Chem. 23 (2019) 1738–1755.
[18] H.Y. Gondal, Z.M. Cheema, H. Siddiqui, et al., Facile efficient synthesis of new alkoxymethylphosphonium tetrafluoroborates; Valuable alternative to their halide analogues, Chem. Afr. 1 (2018) 97–102.
[19] H.Y. Gondal, Z.M. Cheema, J.H. Zaidi, et al., Facile synthesis of α-alkoxymethyltriphenylphosphonium iodides: new application of PPh 3/I 2, Chem. Cent. J. 12 (2018) 1–10.
[20] H.Y. Gondal, S. Mumtaz, A. Abbaskhan, et al., New alkoxymethyl-functionalized pyridinium-based chiral ionic liquids: Synthesis, characterization and properties, Chem. Pap. 74 (2020) 2951–2963.
[21] S. Mumtaz, I. Cano, N. Mumtaz, et al., Supramolecular interaction of non-racemic benzimidazolium based ion pairs with chiral substrates, PCCP 20 (2018) 20821–20826.
[22] M. Nisar, H.Y. Gondal, Z.M. Cheema, et al., Lewis acid-catalyzed synthesis of alkoxymethylhalides for multipurpose mixed acetals; Scope and limitations, Lett. Org. Chem. 19 (2022) 750–756.
[23] M. Nisar, H.Y. Gondal, Z.M. Cheema, et al., New azole-derived hemiaminal ethers as promising acetylcholinesterase inhibitors: synthesis, X-ray structures, in vitro and in silico studies, J. Biomol. Struct. Dyn. (2023) 1–14.
[24] F.A. Larik, M.S. Shah, A. Saeed, et al., New cholinesterase inhibitors for Alzheimer's disease: Structure activity relationship, kinetics and molecular docking studies of 1–butanoyl–3–arylthiourea derivatives, Int. J. Biol. Macromol. 116 (2018) 144–150.
[25] Le Berre, M., J. Q. Gerlach, I. Dziembała, et al., 2022. Calculating Half Maximal Inhibitory Concentration (IC 50) Values from Glycomics Microarray Data Using GraphPad Prism. Glycan Microarrays: Methods and Protocols. 89-111.
[26] Studio, D., Discovery studio. Accelrys [2.1] 2008.
[27] Huey, R.; Morris, G. M., Using AutoDock 4 with AutoDocktools: a tutorial. The Scripps Research Institute, USA 2008, 8, 54-56.
[28] Y. Liu, X. Yang, J. Gan, S. Chen, Z.-X. Xiao, Y. Cao, CB-Dock 2: Improved protein–ligand blind docking by integrating cavity detection, docking and homologous template fitting, Nucleic Acids Res. 50 (W1) (2022) W159–W164.
[29] P. Banerjee, A.O. Eckert, A.K. Schrey, R. Preissner, ProTox-II: a webserver for the prediction of toxicity of chemicals, Nucleic Acids Res. 46 (W1) (2018) W257–W263.
[30] A. Daina, O. Michielin, V. Zoete, SwissADME: a free web tool to evaluate pharmacokinetics, drug-likeness and medicinal chemistry friendliness of small molecules, Sci. Rep. 7 (1) (2017) 42717.
[31] D.E. Pires, T.L. Blundell, D.B. Ascher, pkCSM: predicting small-molecule pharmacokinetic and toxicity properties using graph-based signatures, J. Med. Chem. 58 (9) (2015) 4066–4072.
[32] DeLano, W. L., Pymol: An open-source molecular graphics tool. CCP4 Newsl. Protein Crystallogr 2002, 40 (1), 82-92.
[33] V. Zoete, M.A. Cuendet, A. Grosdidier, O. Michielin, SwissParam: a fast force field generation tool for small organic molecules, J. Comput. Chem. 32 (11) (2011) 2359–2368.
[34] C. Kutzner, C. Kniep, A. Cherian, L. Nordstrom, H. Grubmüller, B.L. de Groot, V. Gapsys, GROMACS in the cloud: A global supercomputer to speed up alchemical drug design, J. Chem. Inf. Model. 62 (7) (2022) 1691–1711.
[35] W. Humphrey, A. Dalke, K. Schulten, VMD: visual molecular dynamics, J. Mol. Graph. 14 (1) (1996) 33–38.
[36] E.F. Pettersen, T.D. Goddard, C.C. Huang, G.S. Couch, D.M. Greenblatt, E.C. Meng, T.E. Ferrin, UCSF Chimera—a visualization system for exploratory research and analysis, J. Comput. Chem. 25 (13) (2004) 1605–1612.